PAPER • **OPEN ACCESS**

The gap size effect on leakage flow and cavitation in the clearance of a 2D hydrofoil: high-speed visualization and velocity measurements

To cite this article: Konstantin S Pervunin *et al* 2019 *IOP Conf. Ser.: Earth Environ. Sci.* **240** 062040

View the article online for updates and enhancements.

This content was downloaded from IP address 159.226.140.26 on 08/10/2019 at 01:35

The gap size effect on leakage flow and cavitation in the clearance of a 2D hydrofoil: high-speed visualization and velocity measurements

Konstantin S Pervunin[1,*], Mikhail V Timoshevskiy[1], Ivan I Zapryagaev[1], Dmitriy M Markovich[1,2,3], Georgy A Semenov[4] and Aleksandr V Zakharov[4]

[1] Kutateladze Institute of Thermophysics, Siberian Branch of the Russian Academy of Sciences, 1, Lavrentyev Ave., Novosibirsk, 630090, Russia
[2] Department of Physics, Novosibirsk State University, 2, Pirogov Str., Novosibirsk, 630090, Russia
[3] Institute of Power Engineering, Tomsk Polytechnic University, 30, Lenin Ave., Tomsk, 634050, Russia
[4] Public Joint-Stock Company "Power Machines" (LMZ), 3A, Vatutin Str., Saint-Petersburg, 195009, Russia

[*]pervunin@itp.nsc.ru

Abstract. In the study, tip-clearance cavitation inception and development was studied in the gap between an end face of a NACA0022-34 hydrofoil and a transparent sidewall of a test channel. The experiments were carried out for the attack angles of 3º and 9º and the gap width of 0.4 to 0.8 mm under various flow conditions on the cavitation number. In order to observe the tip-clearance cavitation inception and its dynamics, a high-speed visualization was applied. The leakage flow velocity was measured inside the clearance by a modified PTV technique. It was shown that unsteady dynamics of the primary cavity on the foil suction side affects the leakage flow direction and the gap cavitation evolution. An increase of the gap width causes the gap cavitation to be initiated at higher cavitation numbers.

1. Introduction

One of the most widespread forms of cavitation in hydraulic machinery is so called tip-clearance cavitation that occurs in narrow channels. The tip-clearance cavitation is frequently observed in the gaps between tip edges of rotor blades or end faces of guide vanes and stator housing. The most destructive impact of this type of cavitation is observed on operating elements of hydraulic equipment where the flow leaking through a slot channel comes out to the suction side of a hydrofoil. Distinctive features of tip-leakage flow are as follows:
- relatively low spatial scale varying from several fractions of a millimeter to several millimeters;
- high shear rate produced by a considerable velocity of the leakage flow itself and the relative motion of walls forming a clearance;
- strong vorticity generated by the leakage flow where it escapes a gap to the suction side of a blade.

These particular features, however, make it difficult to investigate tip-leakage flow and associated tip-clearance cavitation both experimentally and numerically.

Content from this work may be used under the terms of the Creative Commons Attribution 3.0 licence. Any further distribution of this work must maintain attribution to the author(s) and the title of the work, journal citation and DOI.
Published under licence by IOP Publishing Ltd

In the literature, the tip-clearance cavitation is further classified into three main subtypes:
- gap cavitation occurring in a clearance due to separation of the leakage flow from a vane end face;
- tip-leakage vortex (TLV) cavitation induced by an interaction of the leakage flow with the primary one when the former comes out to the suction side [1–4];
- tip-separation vortex (TSV) cavitation caused by the leakage flow separation and its further turbulization inside a clearance [5–7].

These vortices and cavities interplay in a complex manner with one another and with the primary cavity flow, making the vortex structure of the secondary flow very complicated. This paper aims at an experimental investigation of a tip-clearance cavitation and tip-leakage flow structure within the gap formed by a channel sidewall and 2D hydrofoil end face. In the experiments, a PIV technique adapted for velocity measurements in slot channels and high-speed visualization were used. The study is carried out for the attack angles of 3° and 9° and various cavitation regimes.

2. Experimental setup and measurement techniques

The experiments were conducted in the cavitation tunnel in Kutateladze Institute of Thermophysics SB RAS which test section is a 1.3 m long channel of *a*x*b* = 80x250 mm rectangular cross-section equipped with transparent windows. The experimental rig, flow conditions, measurement techniques and data-processing procedures are described in detail in [8]. A NACA0022-34 section which profile is close to the one of guide vanes (GV) of a Francis turbine was used as a test object. The foil chord length is C = 100 mm, with the maximum thickness of H^{max}/C = 0.22 reached at the distance of x^{max}/C = 0.4 from the leading edge. The rotation axis positioned in the foil geometric center is of 21.1 mm diameter and, thus, does not go beyond the generatrix of the GV model profile (Figure 1-a). In the present research, the clearance width h was set to be 0.4 mm and 0.8 mm (Figure 1-b). In order to change the gap size, the hydrofoil has a composite construction: it consists of the main body of 65 mm width and two end plates of different widths (14 and 14.4 mm) that replicate the foil shape and are attached to the main body (see an example in Figure 1).

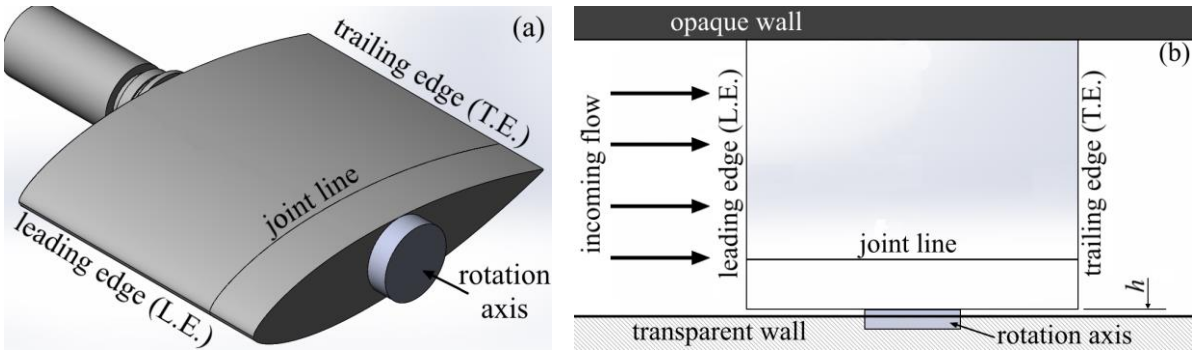

Figure 1. (a) 3D model of the NACA0022-34 hydrofoil with the axis of rotation on both end faces and (b) schematic of its disposition in the test section (top view). The joint line denotes a line along which the foil main body and the end plates are connected. h is the gap width.

The investigation was performed for the attack angle α = 3° and 9°. Different flow conditions were achieved by varying the cavitation number $\sigma = (p_{in}-p_V)/(\rho U_0^2/2)$ in the range from 1.74 to 0.79 for α = 3° and from 3.97 to 1.31 for α = 9° by changing the mean flow velocity U_0 from 7.75 to 12.99 m/s. Here, p_V is the saturation vapor pressure of the operating liquid (distilled water), ρ is the liquid density and p_{in} is the static pressure equaled to 50 kPa that was gauged by a pressure transducer at a sidewall close to the test section inlet. U_0 was measured by PIV in the central longitudinal plane of the test section far upstream of the hydrofoil location. The Reynolds number $\mathrm{Re} = CU_0/\nu$, where ν is the kinematic viscosity of the operating liquid, equaled to $1.3\cdot10^6 – 1.6\cdot10^6$ for α = 3° and $0.97\cdot10^6 – 1.44\cdot10^6$ for α = 9°. In order to measure the leakage flow velocity within the gap the following measurement system was used. The operating liquid was seeded with PMMA fluorescent particles of

Microparticles GmbH production filled with Rhodamine B (fraction 1-20 μm). The gap was illuminated with a laser beam expanded by means of Edmund Optics 2-8X 532 nm beam expander to cover the whole foil end face with the axis. A camera equipped with a low-pass optical filter to block the laser light was installed normally to the GV end surface while the laser beam was inclined at the angle of nearly 45° to the camera line of sight. The tracer displacements were determined by a relaxation PTV approach [9].

3. Results

3.1. High-speed visualization

3.1.1. Small gap size (0.4 mm). At the low attack angle α = 3°, cavitation is first initiated at σ = 1.05 as isolated cavities inside the tip-leakage vortex (TLV) originating downstream of the hydrofoil axis. It is worth noting that, in the present configuration of the GV model, the leakage flow is separated by the axis into two parts – nose and aft ones – in which the flow develops almost independently. That is why TLV is present in both of them. When the cavitation number is decreased to σ = 1 (Figure 2-a), the cavitating core of the aft TLV becomes more pronounced and the nose TLV also cavitates in the same manner closer to the foil axis. In addition, cavitation also occurs inside a vortex that arises due to separation of the leakage flow from the axis in the nose part, hereinafter it is referred to as axis-separation vortex. In this study, the tip-separation vortex was not registered due apparently to the presence of the foil axis and the axis-separation vortex seems to appear instead. On the GV suction side, transient bubble cavitation begins. A further reduction of the cavitation number to σ = 0.95 leads to transformation of the cavitating flow regime to a transitional one that is characterized by a quite dense concentration of the traveling bubbles on the foil suction side, which is the reason why the bubbles start to interact with one another and merge downstream forming a bubbly cavity with the streamwise dimension L_C/C = 0.49. The cavitation in the vortices turns out to be also more intense. In the clearance, gap cavitation appears occasionally in form of a sheet cavity near the foil leading edge (Figure 2-b).

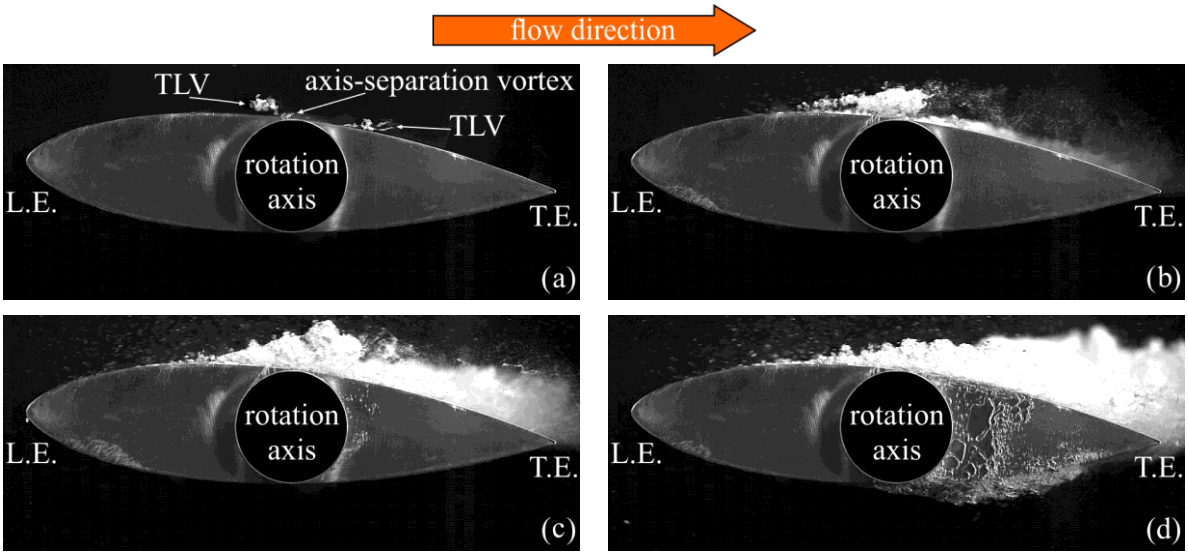

Figure 2. Instantaneous images (side view) of tip-clearance cavitation in the gap between the GV end face and the test section sidewall for h = 0.4 mm and α = 3° when (a) σ = 1, (b) σ = 0.95, (c) σ = 0.9 and (d) σ = 0.79.

At σ = 0.9 (Figure 2-c), the primary cavity on the GV suction side becomes long enough (L_C/C = 0.62) to be sensitive to local pressure fluctuations and, thus, the flow regime undergoes a transition to

cavitation surge. The sheet cavity in the clearance somewhat elongates and a cavitating axis-separation vortex additionally appears in the aft part closer to the pressure side. Finally, when σ equals to 0.79 (Figure 2-d), the main cavity with L_C/C = 0.73 is absolutely unsteady and oscillates at the reduced frequency St = fL_C^{max}/U_0 = 0.12. Depending upon the stage of the primary cavity evolution, the gap cavitation pattern and the leakage flow direction also change. The former vanishes completely and is the most intense when cavitation on the GV suction side is practically absent and the most pronounced, though the primary cavity is already breaking down (i.e. its length is not maximum). The latter is directed upward (i.e. from the pressure side to the suction one) and downward when the main cavity grows and diminishes, respectively. At the moment of the most developed gap cavitation, the nose sheet cavity turns out to be even smaller than that at σ = 0.9 (Figure 2-c) but, in the aft part of the clearance, a bubbly cavity expands substantially right behind the hydrofoil axis. Moreover, an intensive cavitating tip-leakage vortex is present on the pressure side.

At the higher inclination α = 9°, cavitation starts to develop in the clearance at σ = 2.37 in form of a sheet cavity near the GV leading edge but is still unstable and randomly disappears (Figure 3-a). The major cavity on the suction side is absent and originates as individual traveling bubbles only at σ = 1.93. A decrease in the cavitation number to σ = 1.75 results in an elongation of the sheet cavity in the clearance and modification of its structure to a streaky one (Figure 3-b). Besides, the tip-leakage vortex core begins to cavitate and a sheet cavity is sporadically initiated in a narrow region on the GV suction side adjacent to the gap. The cavity in the clearance changes its length continuously and irregularly, provoking the suction side cavity onset when it reaches the foil edge adjoining to the suction side. The transient bubbles on the foil suction side enlarge and have distinct streamers that indicate to their interaction with turbulent boundary layer. When σ = 1.66 (Figure 3-c), the flow regime becomes transitional and the primary cavity of L_C/C = 0.47 having a bubbly structure is formed on the suction side over the whole foil span. A transition to unsteady flow conditions occurs at σ = 1.51 (Figure 3-d), with the maximum length of the main cavity increased to L_C^{max}/C = 0.62 and the frequency of the cavity auto-oscillations being St = 0.1. At this regime, a cavitating axis-separation vortex appears in the nose part of the clearance and elongated transient bubbles originate immediately behind the axis (i.e. in the gap aft part).

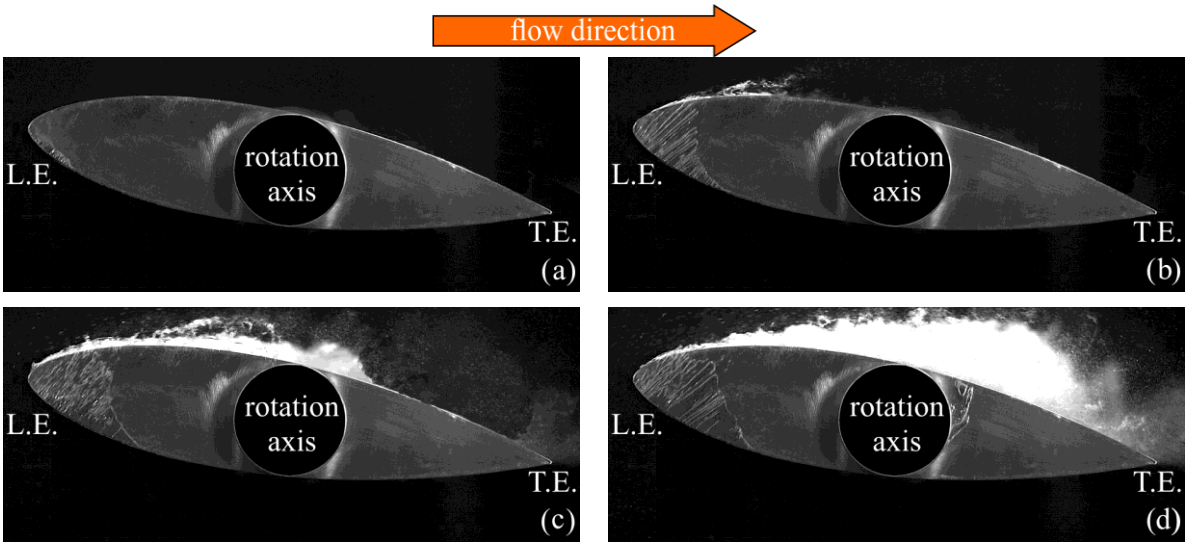

Figure 3. Instantaneous images (side view) of tip-clearance cavitation in the gap between the GV end face and the test section sidewall for h = 0.4 mm and α = 9° when (a) σ = 2.37, (b) σ = 1.75, (c) σ = 1.66 and (d) σ = 1.51.

3.1.2. Large gap size (0.8 mm). An increase of the gap width to h = 0.8 mm leads to an earlier onset of cavitation in the clearance (i.e. at higher cavitation numbers) but the evolution of the suction side

cavitation remains almost unchanged. For instance, at α = 3°, the tip-leakage vortices are already prone to cavitation when σ = 1.3. At σ = 0.95, a transitional cavitation regime of the primary cavity (L_C/C = 0.51) is also observed but the sheet cavity in the gap turns out to be in general longer by 50% than that for h = 0.4 mm (cf. Figures 2-b and 4-a). Transition to the cavitation surge conditions occurs at σ = 0.87 (St = 0.1), which is very close to the case with h = 0.4 mm. However, the gap cavitation appears again to be more developed for h = 0.8 mm (the sheet cavity length is increased by roughly 50%, cf. Figures 2-c and 4-b), with a sheet cavity arisen behind the foil axis. For the higher incidence angle (α = 9°), a sheet cavity is initiated at σ = 2.75 in the clearance close to the GV leading edge. A pronounced cavitating core of the tip-leakage vortex becomes visible when σ = 1.75. At σ = 1.66, a transitional cavity of L_C/C = 0.4 is formed on the suction side and the gap cavity covers more than a half of the nose part of the clearance while the one for h = 0.4 mm occupies only one third of that area (cf. Figures 3-c and 4-c). The primary cavity with L_C/C = 0.7 becomes unsteady (St = 0.11) when σ = 1.44, which is a bit lower than for h = 0.4 mm (Figure 4-d).

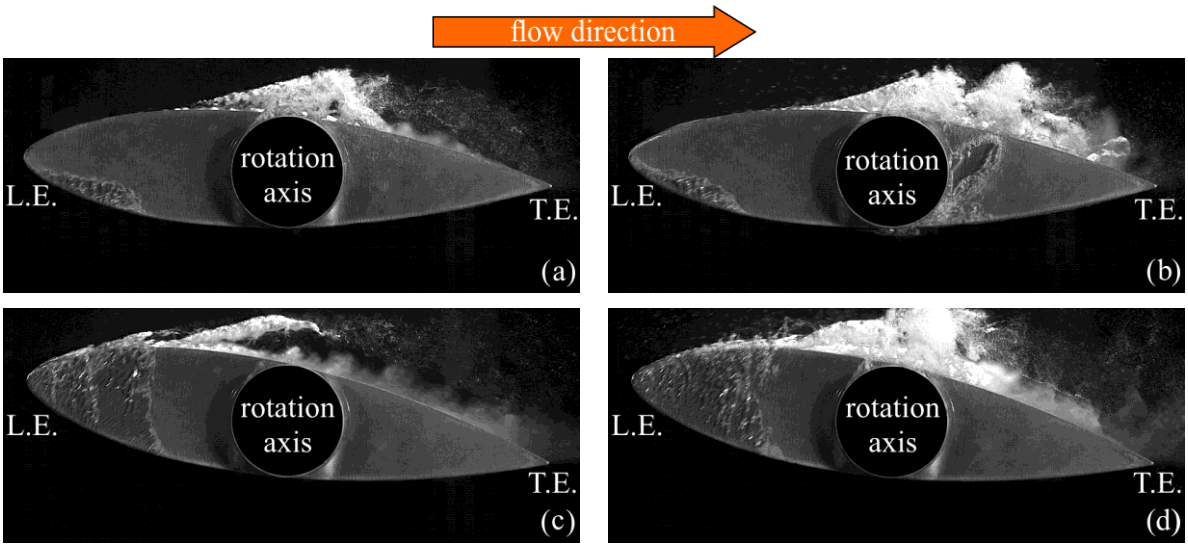

Figure 4. Instantaneous images (side view) of tip-clearance cavitation in the gap between the GV end face and the test section sidewall for h = 0.8 mm when (a) α = 3° and σ = 0.95, (b) α = 3° and σ = 0.87, (c) α = 9° and σ = 1.66 and (d) α = 9° and σ = 1.44.

3.2. Velocity measurements

The velocity measurements were carried out for the following flow conditions: subcavitating flow, steady tip-clearance cavitation and unsteady cavitation surge conditions (Figure 5). As seen, the mean velocity distributions for all these cases are not uniform. For example, when the gap cavitation in form of a sheet cavity occurs near the GV leading edge (zone I in Figure 5-b and 5-c), the flow velocity in this region rises up to $1.55U_0$ due to a contraction of the gap width by the cavity. In this zone, the velocity for the unsteady flow conditions (Figure 5-c) turns out to be somewhat smaller as compared to that for the regime with the steady gap cavitation (Figure 5-b) because of induced pulsations by the primary flow. Zone II in Figure 5 shows a region of the leakage flow in the nose part of the clearance where it is directed almost upward and takes values in the range between $0.7U_0$–$1.2U_0$. Immediately behind the GV rotation axis, there exist two recirculation zones marked as III and IV (Figure 5), where the leakage flow velocity is very low (about $0.1U_0$). Zone IV is a dead region while zone III is adjacent to the main flow over the foil suction side and, thus, influenced by it. Finally, in zone V (Figure 5), the leakage flows is also directed upstream as in zone II but its velocity is substantially reduced ($0.5U_0$–$0.9U_0$). It is worth noting that the measured velocity distributions of the leakage flow are weakly dependent on the primary flow regime.

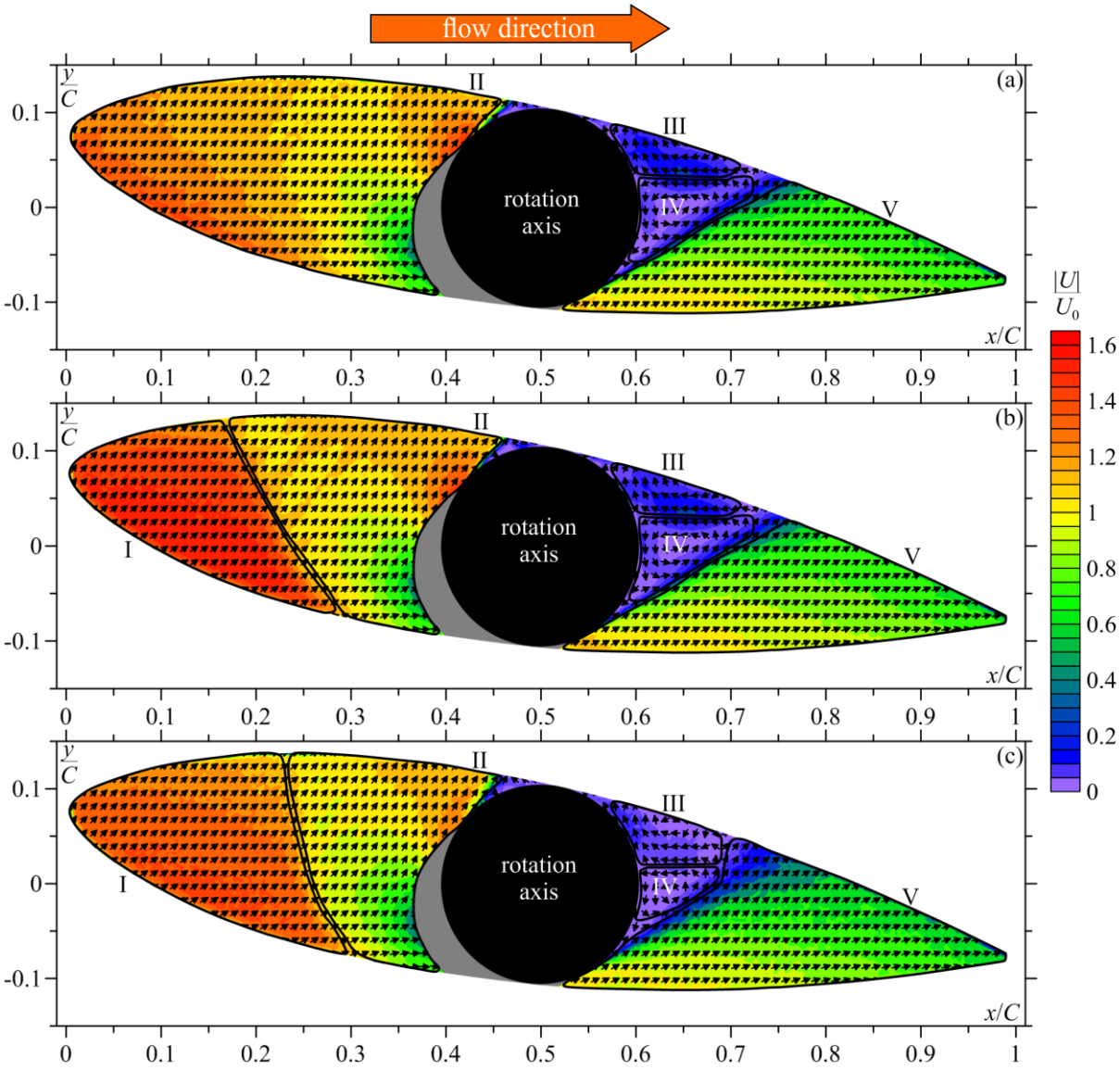

Figure 5. Plane distributions of the time-averaged velocity (absolute values) in the clearance between the GV end face and the test section sidewall for h = 0.8 mm and α = 9° when (a) σ = 3.97 (subcavitating flow), (b) σ = 1.75 (steady tip-clearance cavitation) and (c) σ = 1.37 (cavitation surge). The black circle depicts the GV rotation axis and the grey area indicates its shadow when illuminated by a laser. The velocity fields are separated into several distinct zones corresponding to I – gap cavitation (if it is the case), II – preaxial upward flow, III and IV – clockwise and counterclockwise recirculation zones behind the axis and V – upward flow in the aft part of the clearance.

4. Conclusions

Using a high-speed imaging and PTV approach, the inception and evolution of tip-clearance cavitation was investigated on a NACA0022-34 hydrofoil representing a scaled-down model of guide vanes of a Francis turbine for the attack angle of 3° and 9° and the gap width of 0.4 and 0.8 mm. It was shown that an increase of the gap size causes the tip-clearance cavitation to occur at higher cavitation numbers or, in other words, the wider the gap is, the more prone to cavitation the tip-leakage flow. In addition, unsteady dynamics of the primary cavity on the foil suction side was revealed to strongly influence the direction of the leakage flow and the gap cavitation evolution, depending upon the phase of the cavity growth/reduction cycle. The velocity distributions in the clearance are divided into five

characteristic zones where the direction and velocity of the leakage flow change noticeably. However, they are almost independent of the main flow regime.

Acknowledgments
The research was funded by a grant from the Russian Foundation for Basic Research (Project No. 17-08-01199). The measurement equipment and experimental facilities were provided by the Ministry of Science and Higher Education of the Russian Federation.

References
[1] McCormick Jr B W 1962 On cavitation produced by a vortex trailing from a lifting surface *ASME J. Basic Eng.* **84(3)** 369–378
[2] Arndt R E A, Arakeri V H and Higuchi H 1991 Some observations of tip-vortex cavitation *J. Fluid Mech.* **229** 269–289
[3] Boulon O, Callenaere M, Franc J-P and Michel J-M 1999 An experimental insight into the effect of confinement on tip vortex cavitation of an elliptical hydrofoil *J. Fluid Mech.* **390** 1–23
[4] Pennings P, Westerweel J and van Terwisga T 2016 Cavitation tunnel analysis of radiated sound from the resonance of a propeller tip vortex cavity *Int. J. Multiphase Flow* **83** 1–11
[5] Zhao Y, Wang G, Jiang Y and Huang B 2016 Numerical analysis of developed tip leakage cavitating flows using a new transport-based model *Int. Commun. Heat Mass Trans.* **78** 39–47
[6] Guo Q, Zhou L and Wang Z 2016 Numerical evaluation of the clearance geometries effect on the flow field and performance of a hydrofoil *Renew. Energy* **99** 390–397
[7] Wang B-L, Liu Z-H, Li H-Y, Wang Y-Y, Liu D-C, Zhang L-X and Peng X-X 2017 On the numerical simulations of vortical cavitating flows around various hydrofoils *J. Hydrodyn.* **29(6)** 926–938
[8] Kravtsova A Yu, Markovich D M, Pervunin K S, Timoshevskiy M V and Hanjalić K 2014 High-speed visualization and PIV measurements of cavitating flows around a semi-circular leading-edge flat plate and NACA0015 hydrofoil *Int. J. Multiphase Flow* **60** 119–134
[9] Baek S J, Lee S J 1996 A new two-frame particle tracking algorithm using match probability *Exp Fluids* **22(1)** 23–32